Inorganic Chemistry

Article

pubs.acs.org/IC

Carbonato-Bridged $Ni^{II}_2Ln^{III}_2$ (Ln^{III} = Gd^{III}, Tb^{III}, Dy^{III}) Complexes Generated by Atmospheric CO_2 Fixation and Their Single-Molecule-Magnet Behavior: $[(\mu_4\text{-}CO_3)_2\{Ni^{II}(3\text{-MeOsaltn})(MeOH \text{ or } H_2O)Ln^{III}(NO_3)\}_2]\cdot$solvent [3-MeOsaltn = *N*,*N*′-Bis(3-methoxy-2-oxybenzylidene)-1,3-propanediaminato]

Soichiro Sakamoto,[†] Takeshi Fujinami,[†] Koshiro Nishi,[†] Naohide Matsumoto,*[,†] Naotaka Mochida,[‡] Takayuki Ishida,[‡] Yukinari Sunatsuki,[§] and Nazzareno Re[∥]

[†]Department of Chemistry, Faculty of Science, Kumamoto University, Kumamoto 860-8555, Japan

[‡]Department of Engineering Science, The University of Electro-Communications, Chofu, Tokyo 182-8585, Japan

[§]Department of Chemistry, Faculty of Science, Okayama University, Tsushima-naka 3-1-1, Okayama 700-8530, Japan

[∥]Facolta di Farmacià, Universita degli Studi "G. D. Annunzio", I-66100 Chieti, Italy

Supporting Information

ABSTRACT: Atmospheric CO_2 fixation of $[Ni^{II}(3\text{-MeOsaltn})(H_2O)_2]\cdot 2.5H_2O$ [3-MeOsaltn = *N*,*N*′-bis(3-methoxy-2-oxybenzylidene)-1,3-propanediaminato], $Ln^{III}(NO_3)_3\cdot 6H_2O$, and triethylamine occurred in methanol/acetone, giving a first series of carbonato-bridged $Ni^{II}_2Ln^{III}_2$ complexes $[(\mu_4\text{-}CO_3)_2\{Ni^{II}(3\text{-MeOsaltn})(MeOH)\text{-}Ln^{III}(NO_3)\}_2]$ (**1Gd**, **1Tb**, and **1Dy**). When the reaction was carried out in acetonitrile/water, it gave a second series of complexes $[(\mu_4\text{-}CO_3)_2\{Ni^{II}(3\text{-MeOsaltn})(H_2O)\text{-}Ln^{III}(NO_3)\}_2]\cdot 2CH_3CN\cdot 2H_2O$ (**2Gd**, **2Tb**, and **2Dy**). For both series, each $Ni^{II}_2Ln^{III}_2$ structure can be described as two di-μ-phenoxo-bridged $Ni^{II}Ln^{III}$ binuclear units bridged by two carbonato CO_3^{2-} units to form a carbonato-bridged $(\mu_4\text{-}CO_3)_2\{Ni^{II}_2Ln^{III}_2\}$ structure. The high-spin Ni^{II} ion has octahedral coordination geometry, and the Ln^{III} ion is coordinated by O_9 donor atoms from Ni^{II}(3-MeOsaltn), bidentate NO_3^-, and one and two oxygen atoms of two CO_3^{2-} ions. The NO_3^- ion for the first series roughly lie on Ln−O(methoxy) bonds and are tilted toward the outside, while for the second series, the two oxygen atoms roughly lie on one of the Ln−O(phenoxy) bonds due to the intramolecular hydrogen bond. The temperature-dependent magnetic susceptibilities indicated a ferromagnetic interaction between the Ni^{II} and Ln^{III} ions (Ln^{III} = Gd^{III}, Tb^{III}, Dy^{III}) for all of the complexes, with a distinctly different magnetic behavior between the two series in the lowest-temperature region due to the Ln^{III}−Ln^{III} magnetic interaction and/or different magnetic anisotropies of the Tb^{III} or Dy^{III} ion. Alternating-current susceptibility measurements under the 0 and 1000 Oe direct-current (dc) bias fields showed no magnetic relaxation for the $Ni^{II}_2Gd^{III}_2$ complexes but exhibited an out-of-phase signal for $Ni^{II}_2Tb^{III}_2$ and $Ni^{II}_2Dy^{III}_2$, indicative of slow relaxation of magnetization. The energy barriers, Δ/k_B, for the spin flipping were estimated from the Arrhenius plot to be 12.2(7) and 6.1(3) K for **1Tb** and **2Tb**, respectively, and 18.1(6) and 14.5(4) K for **1Dy** and **2Dy**, respectively, under a dc bias field of 1000 Oe. Compound **1Dy** showed relatively slow relaxation of magnetization reorientation even at zero dc applied field with Δ/k_B = 6.6(4) K.

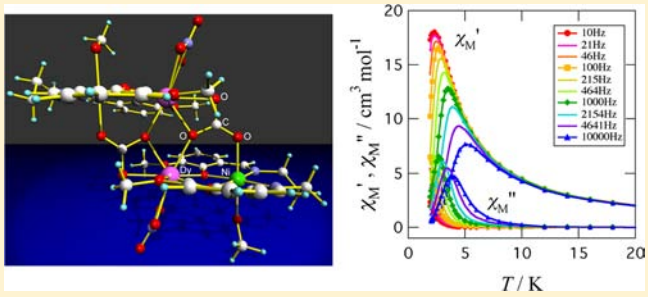

INTRODUCTION

The fixation of atmospheric CO_2 (ca. 0.03% in air) and its conversion into useful chemical compounds by metal complexes under mild conditions are of continuous attention and a challenge to the chemists to reduce serious environmental problems.[1] Metalloenzymes like carbonic anhydrase and nonheme iron in the photosynthetic system II are well-known to have a pivotal role in the activation and fixation of CO_2.[2] Spontaneous fixation of atmospheric CO_2 by coordination compounds is rare because of its low concentration in air and its high thermodynamic stability. In most cases, the carbonate complexes were obtained by the addition of Na_2CO_3, or $NaHCO_3$, or bubbling CO_2 to the reaction solution.[3] Several examples of CO_2 fixation from air have been reported for transition-metal complexes.[4] Transition-metal complexes such as $[(Cu^I\{HB(3,5\text{-}Pr_2pz)_3\})_2(OH)_2]$ [$HB(3,5\text{-}Pr_2pz)_3$ = hydrotris(3,5-diisopropylpyrazol-1-yl)borate],[4a] $[Ni^{II}(N,N\text{-}Me_2en)_3](ClO_4)_2$ (*N*,*N*-Me_2en = *N*,*N*-dimethylethylenediamine),[4b] and $[Zn^{II}_2L]^{2+}$ (L = octaazacryptate)[4c] were shown to fix

Received: April 4, 2013
Published: May 24, 2013

   dx.doi.org/10.1021/ic4008312 | *Inorg. Chem.* 2013, 52, 7218−7229

Scheme 1. Possible Reaction Route to the Carbonato-Bridged $Ni^{II}_2Ln^{III}_2$ Complex $[(\mu_4\text{-}CO_3)_2\{Ni^{II}(3\text{-}MeOsaltn)(MeOH)Ln^{III}(NO_3)\}_2]$

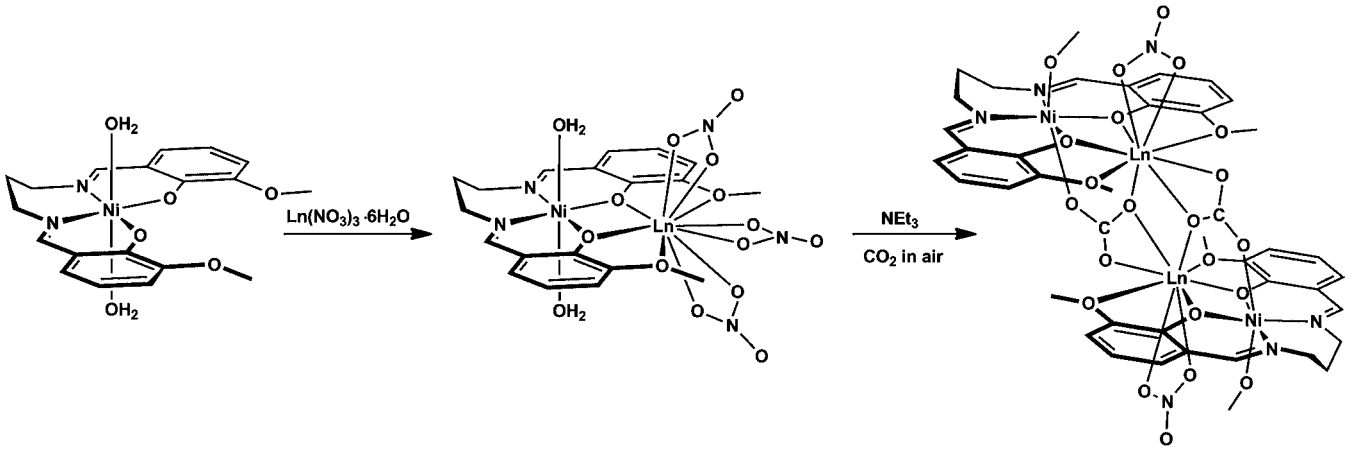

atmospheric CO_2 to produce carbonato-bridged binuclear complexes. Recently, several carbonato-bridged lanthanide clusters generated by atmospheric CO_2 fixation were reported, and some of them were studied from the viewpoints of single-molecule magnets (SMMs).[5] To the best of our knowledge, there are no reports of 3d−4f complexes having been used for CO_2 fixation. We report here the first example of atmospheric CO_2 fixation by 3d−4f complexes and SMM behaviors.

The carbonato-bridged 3d−4f complexes generated by atmospheric CO_2 fixation were found in the course of our studies on 3d−4f SMMs.[6] We have synthesized a series of 3d−4f binuclear complexes, $[M^{II}(3\text{-}MeOsaltn)(ac)(MeOH)_xLn^{III}(hfac)_2]$ (x = 0 for M = Cu^{II}, Zn^{II}; x = 1 for M = Co^{II}, Ni^{II}; Ln = Gd^{III}, Tb^{III}, Dy^{III}, La^{III}), where 3-MeOsaltn, ac, and hfac denote *N*,*N*′-bis(3-methoxy-2-oxybenzylidene)-1,3-propanediaminato, acetato, and hexafluoroacetylacetonato, respectively.[7] Einaga and co-workers[8a] and Andruh and co-workers[8b] synthesized the 3d−4f binuclear complexes $[Ni^{II}(3\text{-}MeOsaltn)(MeOH)_xLn^{III}(NO_3)_3]$. These 3d−4f binuclear complexes were prepared by mixing the 3d component and the 4f component in a 1:1 molar ratio without the addition of an aqueous NaOH solution or triethylamine, as shown in Scheme 1. We have found that atmospheric CO_2 fixation occurred in a basic reaction mixture of $[Ni^{II}(3\text{-}MeOsaltn)(H_2O)_2]\cdot 2.5H_2O$ and $Ln^{III}(NO_3)_3\cdot 6H_2O$ (Ln^{III} = Gd^{III}, Tb^{III}, Dy^{III}) to produce the carbonato-bridged $Ni^{II}_2Ln^{III}_2$ complexes. When the reaction was carried out in a methanol/acetone solution with the addition of equimolar triethylamine, the first series of complexes with the formula $[(\mu_4\text{-}CO_3)_2\{Ni^{II}(3\text{-}MeOsaltn)(MeOH)Ln^{III}(NO_3)\}_2]$ [Ln^{III} = Gd^{III} (**1Gd**), Tb^{III} (**1Tb**), Dy^{III} (**1Dy**)] was obtained as small-sized crystals. When the reaction was carried out in an acetonitrile/water solution, the second series of complexes with the formula $[(\mu_4\text{-}CO_3)_2\{Ni^{II}(3\text{-}MeOsaltn)(H_2O)Ln^{III}(NO_3)\}_2]\cdot 2CH_3CN\cdot 2H_2O$ [Ln^{III} = Gd^{III} (**2Gd**), Tb^{III} (**2Tb**), Dy^{III} (**2Dy**)] was obtained as well-grown crystals.

These $Ni^{II}_2Ln^{III}_2$ complexes are interesting not only for their atmospheric CO_2 fixation but also because they behave as SMMs. The origin of the SMM behavior is easy-axis magnetic anisotropy (D < 0), which causes formation of an energy barrier that prevents reversal of the molecular magnetization and causes slow relaxation of magnetization at low temperature. SMMs form as a result of the combination of a large-spin multiplicity of the ground state and easy-axis (or Ising-type) magnetic anisotropy of the entire molecule.[9] The first SMM to be discovered was a Mn_{12} cluster,[9] and subsequent efforts led to a number of SMMs consisting of d elements. Syntheses of f complexes[10] and d−f polynuclear complexes[11] are a very promising approach to SMMs. Indeed, (1) a high-spin ground state can be generated by the frequently observed ferromagnetic interaction between d and f elements through the assembly of a smaller number of metal ions than that required for purely d polynuclear complexes and (2) molecular magnetic anisotropy is easily derived from the f component. The two series of present $Ni^{II}_2Ln^{III}_2$ complexes have similar $(\mu_4\text{-}CO_3)_2\{Ni^{II}Ln^{III}\}_2$ structure, but the coordination geometry around the Ln^{III} ion shows a slight difference in the orientation of the NO_3^- ion. The direct-current (dc) magnetic measurements indicate ferromagnetic interaction between the Ni^{II} and Ln^{III} ions and a different magnetic behavior between the two series in the lowest-temperature region. Both series of complexes including the Tb^{III} ($4f^8$, J = 6, S = 3, L = 3, $^7F_6$) and Dy^{III} ($4f^9$, $J = {}^{15}/_2$, $S = {}^5/_2$, L = 5, $^6H_{15/2}$) ions showed slow relaxation processes in the alternating-current (ac) magnetic measurements and slightly different SMM behavior. Here, we report the synthesis, structure, and magnetic properties of the two series of carbonate-bridged $Ni^{II}_2Ln^{III}_2$ complexes generated by spontaneous fixation of CO_2. Part of this study has already been reported.[12]

EXPERIMENTAL SECTION

Materials. All reagents and solvents, obtained from Tokyo Kasei Co. and Wako Pure Chemical Industries, were of reagent grade, and they were used in the syntheses without further purification. All reactions were carried out under an ambient atmosphere.

Component Complex, $[Ni^{II}(3\text{-}MeOsaltn)(H_2O)_2]\cdot 2.5H_2O$. The component Ni^{II} complex $[Ni(3\text{-}MeOsaltn)(H_2O)_2]\cdot 2.5H_2O$ was synthesized according to the method of the literature.[13] Recrystallization was performed from chloroform. Yield: 40%. Anal. Calcd for $C_{19}H_{24}N_2O_6Ni\cdot 2.5H_2O$: C, 47.53; H, 6.09; N, 5.83. Found: C, 47.58; H, 6.06; N, 6.29.

$[(\mu_4\text{-}CO_3)_2\{Ni^{II}(3\text{-}MeOsaltn)(MeOH)Gd^{III}(NO_3)\}_2]$ (1Gd). To a solution of $Gd^{III}(NO_3)_3\cdot 6H_2O$ (45 mg, 0.1 mmol) in 2 mL of MeOH was added a solution of triethylamine (11 mg, 0.1 mmol) at ambient temperature and atmosphere. To the resultant mixture was added a solution of $[Ni(3\text{-}MeOsaltn)(H_2O)_2]\cdot 2.5H_2O$ (48 mg, 0.1 mmol) in 10 mL of MeOH and 5 mL of acetone at room temperature. The color of the mixed solution changed from green to pale green in 10 min. The mixture was filtered, and the filtered clear pale-green solution was left at room temperature under an ambient atmosphere

dx.doi.org/10.1021/ic4008312 | Inorg. Chem. 2013, 52, 7218−7229

Table 1. X-ray Crystallographic Data for $[(\mu_4\text{-}CO_3)_2\{Ni^{II}(3\text{-}MeOsaltn)(MeOH)Ln^{III}(NO_3)\}_2]$ [Ln^{III} = Gd^{III} (1Gd), Tb^{III} (1Tb), Dy^{III} (1Dy)] and $[(\mu_4\text{-}CO_3)_2\{Ni^{II}(3\text{-}MeOsaltn)(H_2O)Ln^{III}(NO_3)\}_2]\cdot 2CH_3CN\cdot 2H_2O$ [Ln^{III} = Gd^{III} (2Gd), Tb^{III} (2Tb), Dy^{III} (2Dy)]

	1Gd	1Tb	1Dy	2Gd	2Tb	2Dy
formula	$C_{21}H_{24}N_3O_{11}GdNi$	$C_{21}H_{24}N_3O_{11}TbNi$	$C_{21}H_{24}N_3O_{11}DyNi$	$C_{22}H_{27}N_4O_{12}GdNi$	$C_{22}H_{27}N_4O_{12}TbNi$	$C_{22}H_{27}N_4O_{12}DyNi$
fw	710.38	712.06	715.63	755.42	757.10	760.67
cryst syst	monoclinic	monoclinic	monoclinic	monoclinic	monoclinic	monoclinic
space group	$P2_1/n$ (No. 14)	$P2_1/n$ (No. 14)	$P2_1/n$ (No. 14)	$P2_1/n$ (No. 14)	$P2_1/n$ (No. 14)	$P2_1/n$ (No. 14)
a, Å	13.859(2)	13.878(2)	13.8684(7)	12.3577(7)	12.3560(7)	12.3437(8)
b, Å	12.034(2)	12.030(2)	12.0541(7)	12.5279(6)	12.5146(7)	12.4100(7)
c, Å	14.012(2)	14.015(2)	14.0314(6)	17.2961(8)	17.267(1)	17.3181(9)
β, deg	91.843(2)	91.984(5)	91.895(2)	101.172(2)	101.211(2)	101.050(2)
V, Å^3	2335.6(4)	2338.3(5)	2344.4(2)	2627.0(2)	2619.1(3)	2603.7(3)
Z	4	4	4	4	4	4
T, K	100	100	100	100	100	100
D_{calcd}, g cm^{-3}	2.020	2.023	2.027	1.910	1.920	1.940
μ, cm^{-1}	36.972	38.671	40.389	32.971	34.625	36.466
R, R_w	0.0713, 0.1781	0.1099, 0.2535	0.0334, 0.1009	0.0349, 0.1190	0.0442, 0.1182	0.0561, 0.1564

for a few days to precipitate small-sized green needle crystals. The crystals are effluorescent to decompose rapidly. They were collected by filtration and dried in vacuo. Yield: 57 mg (40%). Anal. Calcd for $(C_{21}H_{24}N_3O_{11}NiGd)_2\cdot H_2O$: C, 35.06; H, 3.50; N, 5.84. Found: C, 35.19; H, 3.78; N, 6.13. IR (KBr, cm^{-1}): ν(C=N) 1633, $\nu(NO_3^-)$ 1384, $\nu(CO_3)$ 1471, 1440, 740. Thermogravimetric analysis (TGA) for the dried sample: 1.25% is the calculated value of one water molecule per tetramer; 1.35% weight loss in the temperature region lower than 110 °C was observed in the heating process.

$[(\mu_4\text{-}CO_3)_2\{Ni^{II}(3\text{-}MeOsaltn)(MeOH)Tb^{III}(NO_3)\}_2]$ (1Tb). **1Tb** was synthesized in a manner similar to that of **1Gd**, using $Tb(NO_3)_3\cdot 6H_2O$ instead of $Gd(NO_3)_3\cdot 6H_2O$. Pale-green crystals were obtained. Yield: 46 mg (57%). Anal. Calcd for $(C_{21}H_{24}N_3O_{11}NiTb)_2\cdot H_2O$: C, 34.98; H, 3.49; N, 5.83. Found: C, 34.81; H, 3.53; N, 5.82. IR (KBr, cm^{-1}): ν(C=N) 1633, $\nu(NO_3^-)$ 1384, $\nu(CO_3)$ 1471, 1440, 738. TGA: 1.25% is the calculated value of one water per tetramer; 1.34% weight loss in the temperature region lower than 110 °C was observed in the heating process.

$[(\mu_4\text{-}CO_3)_2\{Ni^{II}(3\text{-}MeOsaltn)(MeOH)Dy^{III}(NO_3)\}_2]$ (1Dy). **1Dy** was synthesized in a manner similar to that of **1Gd**, using $Dy(NO_3)_3\cdot 6H_2O$ instead of $Gd(NO_3)_3\cdot 6H_2O$. Pale-green crystals were obtained. Yield: 29 mg (57%). Anal. Calcd for $(C_{21}H_{24}N_3O_{11}NiDy)_2\cdot H_2O$: C, 34.81; H, 3.48; N, 5.80. Found: C, 34.64; H, 3.44; N, 5.92. IR (KBr, cm^{-1}): ν(C=N) 1633, $\nu(NO_3^-)$ 1384, $\nu(CO_3)$ 1471, 1440, 740. TGA: 1.24% is the calculated value to one water per tetramer; 1.30% weight loss in the temperature region lower than 110 °C was observed in the heating process.

$[(\mu_4\text{-}CO_3)_2\{Ni^{II}(3\text{-}MeOsaltn)(H_2O)Gd^{III}(NO_3)\}_2]\cdot 2CH_3CN\cdot 2H_2O$ (2Gd). A solution of $[Ni^{II}(3\text{-}MeOsaltn)(H_2O)_2]\cdot 2.5H_2O$ (48 mg, 0.1 mmol) in 10 mL of MeCN was added to a solution of $Gd(NO_3)_3\cdot 6H_2O$ (45 mg, 0.1 mmol) in 2 mL of MeCN and 2 mL of H_2O. To the resultant mixture was added triethylamine (011 mg, 0.1 mmol) at room temperature under an ambient atmosphere. The color of the mixed solution immediately changed from purple to colorless. The mixture was filtered, and the filtrate, colorless solution, was left at room temperature for several days to precipitate large-sized blue block crystals (see Figure S1 in the Supporting Information). They were collected by filtration and dried in vacuo. Yield: 44 mg. The crystals are effluorescent, and the crystal solvents are easily substituted for the atmospheric water. Anal. Calcd for $(C_{20}H_{22}N_3O_{11}NiGd)_2\cdot CH_3CN\cdot 6H_2O$: C, 32.71; H, 3.86; N, 6.36. Found: C, 32.67; H, 3.77; N, 6.20. IR (KBr, cm^{-1}): ν(C=N) 1633, $\nu(NO_3^-)$ 1384, $\nu(CO_3)$ 1471, 1440, 742.

$[(\mu_4\text{-}CO_3)_2\{Ni^{II}(3\text{-}MeOsaltn)(H_2O)Tb^{III}(NO_3)\}_2]\cdot 2CH_3CN\cdot 2H_2O$ (2Tb). **2Tb** was prepared in the same manner as **2Gd**, using $Tb(NO_3)_3\cdot 6H_2O$ instead of $Gd(NO_3)_3\cdot 6H_2O$.Yield: 42 mg. Anal. Calcd for $(C_{20}H_{22}N_3O_{11}NiTb)_2\cdot 6H_2O$: C, 31.94; H, 3.75; N, 5.58. Found: C, 31.94; H, 3.79; N, 5.85. IR (KBr, cm^{-1}): ν(C=N) 1633, $\nu(NO_3^-)$ 1384, $\nu(CO_3)$ 1471, 1440, 742. TGA: 7.2% is the calculated value of six water molecules per tetramer; 7.6% weight loss in the temperature region lower than 100 °C was observed in the heating process.

$[(\mu_4\text{-}CO_3)_2\{Ni^{II}(3\text{-}MeOsaltn)(H_2O)Dy^{III}(NO_3)\}_2]\cdot 2CH_3CN\cdot 2H_2O$ (2Dy). **2Dy** was prepared in the same manner as **2Gd**, using $Dy(NO_3)_3\cdot 6H_2O$ instead of $Gd(NO_3)_3\cdot 6H_2O$.Yield: 38 mg. Anal. Calcd for $(C_{20}H_{22}N_3O_{11}NiDy)_2\cdot 6H_2O$: C, 31.79; H, 3.73; N, 5.56. Found: C, 31.95; H, 3.84; N, 5.84. IR (KBr, cm^{-1}): ν(C=N) 1633, $\nu(NO_3^-)$ 1384, $\nu(CO_3)$ 1471, 1440, 740.

Physical Measurements. Elemental analyses (C, H, and N) were carried out at the Center for Instrumental Analysis of Kumamoto University. IR spectra were recorded at room temperature using a JEOL JIR-6500W spectrometer with samples in KBr disks. TGA was carried out on a TG/DTA6200 (SII Nano Technology Inc.) instrument at a 5 K min^{-1} heating rate using ca. 5 mg samples. Fast-atom-bombardment mass spectrometry spectra were measured in methanol on a JEOL JMS-700 mass spectrometer; 3-nitrobenzylalcohol was used as the matrix. Temperature-dependent magnetic susceptibilities in the temperature range 1.9−300 K under an external magnetic field of 0.1 T and field-dependent magnetization measurements in an applied magnetic field from 0 to 5 T at 1.9 K were measured with an MPMS XL5 SQUID susceptometer (Quantum Design, Inc.). Microcrystalline samples consisting of Tb^{III} and Dy^{III} ions showed apparent reorientation in the applied magnetic field of 0.1 T. All samples were thus dispersed in liquid paraffin to avoid orientation in the field. The calibrations were performed with palladium. Corrections for diamagnetism were applied using Pascal's constants.[14] The ac magnetic susceptibility was measured on a Quantum Design PPMS ac/dc magnetometer in a temperature range down to 2.0 K under 0 and 1000 Oe dc bias fields.

X-ray Data Collection and Structure Determination. X-ray data were collected on a Rigaku Rapid imaging-plate diffractometer with graphite-monochromated Mo Kα radiation (λ = 0.71069 Å) at 100 K. The first series of complexes of **1Gd**, **1Tb**, and **1Dy** crystallized as small-sized crystals, and it was difficult to grow crystals suitable for the conventional X-ray diffraction apparatus. Because the crystals were effluorescent, a crystal in the reaction vessel was picked up, quickly coated by epoxy resin, and used for the X-ray data collection at 100 K. The second series of complexes of **2Gd**, **2Tb**, and **2Dy** were obtained as large-sized block crystals with dimensions of ca. 3 × 2 × 2 mm^3, and they were also effluorescent. A large-sized crystal was cut to a suitable size, and the crystal was coated by epoxy resin and used for X-ray data collection. The X-ray diffraction data were collected at 100 K. An absorption correction was applied. The data were also corrected for Lorentz and polarization effects. The structures were solved by direct methods and refined on F^2 by a full-matrix least-squares procedure. The crystal structures were determined and refined by direct methods

dx.doi.org/10.1021/ic4008312 | Inorg. Chem. 2013, 52, 7218−7229

Table 2. Coordination Bond Distances (Å) and Angles (deg) and $Ln^{III}\cdots M^{II}$ Distances (Å) with Their Estimated Standard Deviations for the $Ni^{II}_2Ln^{III}_2$ Complexes 1Gd, 1Tb, 1Dy, 2Gd, 2Tb, and 2Dy

	1Gd	1Tb	1Dy	2Gd	2Tb	2Dy
Ln−O1	2.542(7)	2.511(14)	2.518(3)	2.478(3)	2.468(3)	2.440(5)
Ln−O2	2.344(7)	2.320(12)	2.321(4)	2.353(3)	2.334(4)	2.311(5)
Ln−O3	2.358(7)	2.340(13)	2.333(3)	2.315(3)	2.301(4)	2.289(5)
Ln−O4	2.504(7)	2.519(13)	2.487(3)	2.510(3)	2.496(4)	2.486(5)
Ln−O6	2.349(7)	2.344(13)	2.327(3)	2.354(3)	2.343(4)	2.335(5)
Ln−O6*	2.363(7)	2.326(13)	2.322(3)	2.366(3)	2.349(4)	2.327(5)
Ln−O7*	2.462(7)	2.423(14)	2.427(3)	2.434(3)	2.411(4)	2.396(6)
Ln−O8	2.457(8)	2.505(15)	2.442(4)	2.545(3)	2.534(4)	2.520(5)
Ln−O9	2.514(9)	2.476(13)	2.496(4)	2.562(3)	2.554(4)	2.529(6)
Ni−O2	2.036(8)	2.037(14)	2.035(3)	2.067(3)	2.056(4)	2.060(5)
Ni−O3	2.043(7)	2.029(12)	2.055(3)	2.016(3)	2.015(4)	2.011(6)
Ni−O5	2.107(8)	2.110(13)	2.116(3)	2.087(3)	2.089(4)	2.084(6)
Ni−O11	2.192(8)	2.199(12)	2.201(3)	2.137(3)	2.125(4)	2.123(6)
Ni−N1	2.027(9)	2.034(15)	2.027(4)	2.027(4)	2.020(4)	2.024(6)
Ni−N2	2.042(9)	2.018(18)	2.043(4)	2.063(4)	2.051(4)	2.053(6)
Ln···Ni	3.4593(14)	3.450(3)	3.4481(5)	3.4410(6)	3.4346(7)	3.419(1)
Ln···Ln*	3.989	3.969	3.954	4.024	4.002	3.969
Ni−O2−Ln	104.1(3)	104.5(6)	104.4(1)	102.0(1)	102.7(1)	102.8(2)
Ni−O3−Ln	103.4(3)	104.1(6)	103.4(1)	105.0(1)	105.2(1)	105.2(2)
Ln−O6−Ln*	115.7(3)	116.4(6)	116.9(1)	116.5(1)	117.0(1)	116.6(2)

using the *CrystalStructure* crystallographic software package[15] and *SHELXL-97*.[16] A summary of the relevant crystallographic data and the final refinement details of **1Gd**, **1Tb**, **1Dy**, **2Gd**, **2Tb**, and **2Dy** are given in Tables 1 and 2, respectively. All non-hydrogen atoms were refined anisotropically. Hydrogen atoms were calculated and isotropically fixed using the riding model.

RESULTS AND DISCUSSION

Synthesis and Characterization of $Ni^{II}_2Ln^{III}_2$ Complexes (1Gd, 1Tb, and 1Dy) and (2Gd, 2Tb, and 2Dy). The first series of carbonato-bridged tetranuclear $Ni^{II}_2Ln^{III}_2$ complexes (**1Gd**, **1Tb**, and **1Dy**) was synthesized and crystallized from the basic reaction mixture containing $[Ni^{II}(3\text{-MeOsaltn})(H_2O)_2]\cdot 2.5H_2O$, $Ln^{III}(NO_3)_3\cdot 6H_2O$, and triethylamine in a 1:1:1 molar ratio in an acetone/methanol solution (1:2, v/v) at room temperature under an ambient atmosphere. The solution was allowed to stand for a few days, during which time small pale-green crystals precipitated (see Figure S1 in the Supporting Information). The crystal structural analyses confirmed the structure of $[(\mu_4\text{-}CO_3)_2\{Ni^{II}(3\text{-MeOsaltn})(MeOH)Ln^{III}(NO_3)\}_2]$. The crystals absorb the atmospheric water vapor, and elemental analysis agreed with the chemical formula for $\{Ni^{II}(3\text{-MeOsaltn})(MeOH)Ln^{III}(NO_3)(CO_3)\}\cdot 0.5H_2O$. Half a water molecule per [NiLn] unit was detected by TGA. The first series of complexes exhibits carbonate-related IR absorption bands.[3,4,17] The asymmetric ν_3 stretching vibrations of carbonate[17] are observed at 1440 cm^{-1}, and the in-plane ν_4 deformation of $\nu(CO_3)$ is found at 740 cm^{-1}. The IR spectra showed also a characteristic band at 1630 cm^{-1} assignable to a C═N stretching vibration of a Schiff-base ligand and the strong absorptions at 1384 cm^{-1}, due to the presence of the nitrate groups. Single-crystal X-ray analysis, carried out on a single crystal picked up from the reaction solution, confirmed the carbonato-bridged tetranuclear $Ni^{II}_2Ln^{III}_2$ structure of $[(\mu_4\text{-}CO_3)_2\{Ni^{II}(3\text{-MeOsaltn})(MeOH)Ln^{III}(NO_3)\}_2]$.

The second series of $Ni^{II}_2Ln^{III}_2$ complexes (**2Gd**, **2Tb**, and **2Dy**) was similarly synthesized in an acetonitrile/water solution by mixing $[Ni^{II}(3\text{-MeOsaltn})(H_2O)_2]\cdot 2.5H_2O$, $Ln^{III}(NO_3)_3\cdot 6H_2O$, and triethylamine in a 1:1:1 molar ratio at room temperature under an ambient atmosphere. While the mixture was allowed to stand for several days, blue crystals precipitated (see Figure S1 in the Supporting Information). For the second series of $Ni^{II}_2Ln^{III}_2$ complexes, crystals with dimensions of 2 × 2 × 2 mm^3 could be obtained, as shown in the photographs of the crystals, while for the first series of complexes, it was difficult to grow crystals. The crystal structural analyses confirmed the structure of $[(\mu_4\text{-}CO_3)_2\{Ni^{II}(3\text{-MeOsaltn})(H_2O)Ln^{III}(NO_3)\}_2]\cdot 2CH_3CN\cdot 2H_2O$. The crystals were effluorescent because of elimination of acetonitrile as the crystal solvent. Acetonitrile is substituted for the water molecule from vapor. Elemental analyses agreed with the chemical formula of $[(\mu_4\text{-}CO_3)_2\{Ni^{II}(3\text{-MeOsaltn})(H_2O)\text{-}Ln^{III}(NO_3)\}_2]\cdot x CH_3CN\cdot 6H_2O$ (x = 1 for Gd^{III} and x = 0 for Tb^{III} and Dy^{III}). TGA detected the exact number of solvent molecules. The second series of complexes also exhibits characteristic IR bands, similar to those observed for the first series.[17]

It should be noted that the series of carbonato-bridged tetranuclear $Ni^{II}_2Ln^{III}_2$ complexes was obtained when the reaction was carried out under basic reaction conditions with the addition of equivalent triethylamine, while the binuclear $Ni^{II}Ln^{III}$ complexes $[Ni^{II}(3\text{-MeOsaltn})(MeOH)_2Ln^{III}(NO_3)_3]$ were obtained when the reaction was performed without the addition of triethylamine, as reported by Andruh et al.[8b] The detailed investigation on the reaction mechanism of the formation of carbonato-bridged tetranuclear $Ni^{II}_2Ln^{III}_2$ complexes from $[Ni^{II}(3\text{-MeOsaltn})(H_2O)_2]\cdot 2.5H_2O$, $Ln^{III}(NO_3)_3\cdot 6H_2O$, triethylamine, and CO_2 by use of the CO_2 isotope and DFT calculations is underway in our laboratories, and the result will be reported in a separated paper. Here we report the syntheses, structures, and magnetic properties of the carbonato-bridged tetranuclear $Ni^{II}_2Ln^{III}_2$ complexes in their solid states.

Molecular Structures of $Ni^{II}_2Ln^{III}_2$. Two series of $Ni^{II}_2Ln^{III}_2$ complexes, (**1Gd**, **1Tb**, and **1Dy**) and (**2Gd**, **2Tb**, and **2Dy**), have been prepared in two different reaction

dx.doi.org/10.1021/ic4008312 | Inorg. Chem. 2013, 52, 7218−7229

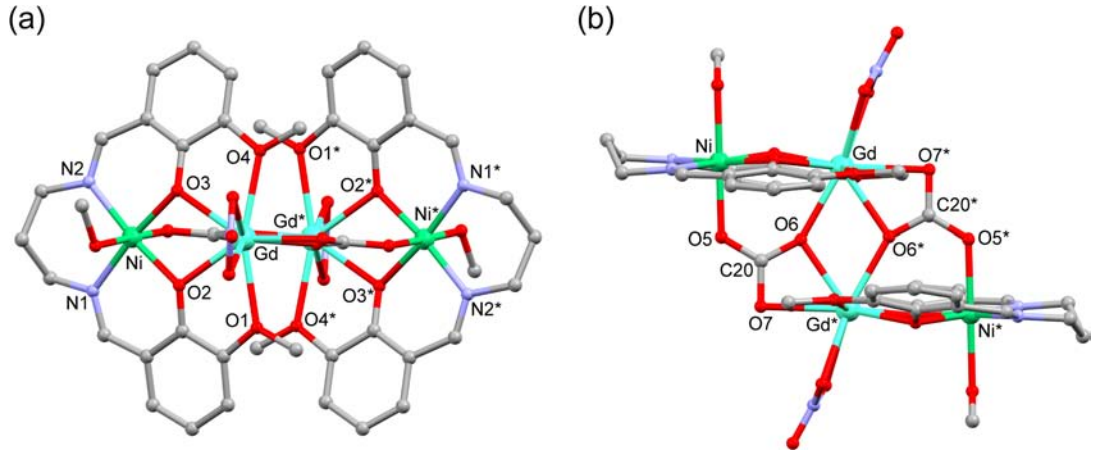

Figure 1. Molecular structures of the tetranuclear $Ni^{II}_2Gd^{III}_2$ complex **1Gd** with the selected atom numbering scheme. The tetranuclear molecule has an inversion center, and the hydrogen atoms are omitted for clarity. (a) Perspective view of **1Gd** projected on the N_2O_2 equatorial coordination planes. (b) Side view showing the $(\mu_4\text{-}CO_3)_2\{Ni^{II}_2Gd^{III}_2\}$ structure and the coordination of the methanol to the Ni^{II} ion and of the chelating nitrate ligand to the Gd^{III} ion.

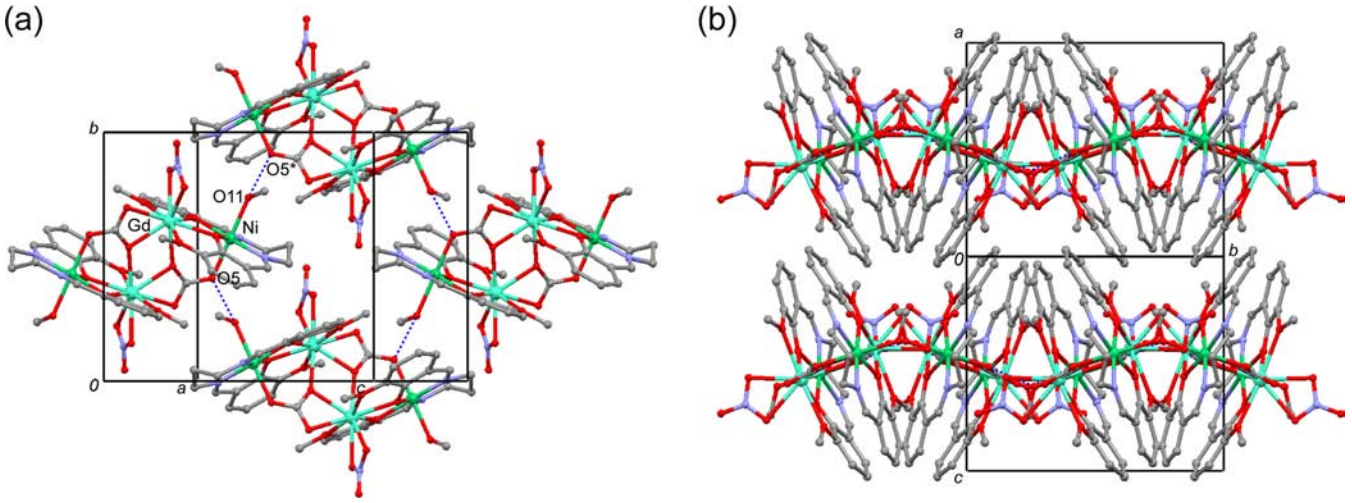

Figure 2. (a) Crystal structure of **1Gd** projected along the *a* axis. (b) Stacking of the adjacent 2D layers of **1Gd**.

solvents; the first series was crystallized in a methanol/acetone solution, while the second series was crystallized in an acetonitrile/water solution. The crystallographic data of the two series of $Ni^{II}_2Ln^{III}_2$ complexes are listed in Table 1. Within each series, the $Ni^{II}_2Ln^{III}_2$ complexes crystallized in the same monoclinic space group $P2_1/n$ (No. 14) with similar cell dimensions, indicating an isomorphous structure. The coordination bond distances and relevant bond angles are listed in Table 2, where the same atom numbering schemes are taken for all six complexes. Because the $Ni^{II}_2Ln^{III}_2$ complexes for each series have isomorphous structure, only the structure of the $Ni^{II}_2Gd^{III}_2$ complexes, **1Gd** and **2Gd**, will be described in detail.

For the first series of $Ni^{II}_2Ln^{III}_2$ complexes (**1Gd**, **1Tb**, and **1Dy**), a crystal was directly picked up from the reaction vessel and was subjected to single-crystal X-ray analysis. The molecular structure of the $Ni^{II}_2Gd^{III}_2$ complex (**1Gd**) with the selected atom numbering scheme is shown in Figure 1a,b, which show a perspective view projected on the N_2O_2 equatorial coordination planes and a side view representing the $(\mu_4\text{-}CO_3)_2$ tetranuclear structure and the coordination mode of the methanol to the Ni^{II} ion and of the nitrate ion to the Gd^{III} ion. The tetranuclear structure, which has an inversion center, can be described as two $[Ni^{II}Gd^{III}]$ binuclear units ($[Ni^{II}(3\text{-}MeOsaltn)(MeOH)Gd^{III}(NO_3)]$, Ni···Gd = 3.459 Å) bridged by two carbonate CO_3^{2-} ions, where the interbinuclear metal···metal distances are Gd···Gd* = 3.989, Ni···Gd* = 5.492, and Ni···Ni* = 8.267 Å (* is the symmetry operation of the inversion center). The binuclear unit consists of a di-μ-phenoxo-bridged structure $Ni^{II}O_2Gd^{III}$ of $[Ni^{II}(3\text{-}MeOsaltn)\text{-}(MeOH)Gd^{III}(NO_3)]$, in which $\{Ni^{II}(3\text{-}MeOsaltn)(MeOH)\}$ acting as a *ligand complex* bridges Ni^{II} and Gd^{III} ions at the two phenoxo and two methoxy groups coordinate to the Gd^{III} ion, leading to a Ni^{II}–Gd^{III} binuclear structure. The dimensions of the bridging $Ni^{II}O_2Gd^{III}$ core are Ni–O2 = 2.036(8) Å, Ni–O3 = 2.043(7) Å, Gd–O2 = 2.344(7) Å, and Gd–O3 = 2.358(7) Å and Ni···Gd = 3.459(1) Å. The Gd–O(methoxy) coordination bond distances [Gd–O1 = 2.542(7) Å and Gd–O4 = 2.504(7) Å] are longer than those of Gd–O(phenoxo) [Gd–O2 = 2.344(7) Å and Gd–O3 = 2.358(7) Å]. In the $(\mu_4\text{-}CO_3)_2$ tetranuclear structure, one carbonate ion (O5, O6, O7, and C20) bridges the Ni^{II} and Gd^{III} ions of a binuclear unit with Ni–O5 = 2.107(8) Å and Gd–O6 = 2.349(7) Å and further coordinates to the Gd^{III} ion of the adjacent binuclear unit as a chelate ligand with Gd*–O6 = 2.363(7) Å and Gd*–O7 = 2.462(7) Å. One carbonato thus acts as a tetradentate ligand

dx.doi.org/10.1021/ic4008312 | *Inorg. Chem.* 2013, 52, 7218–7229

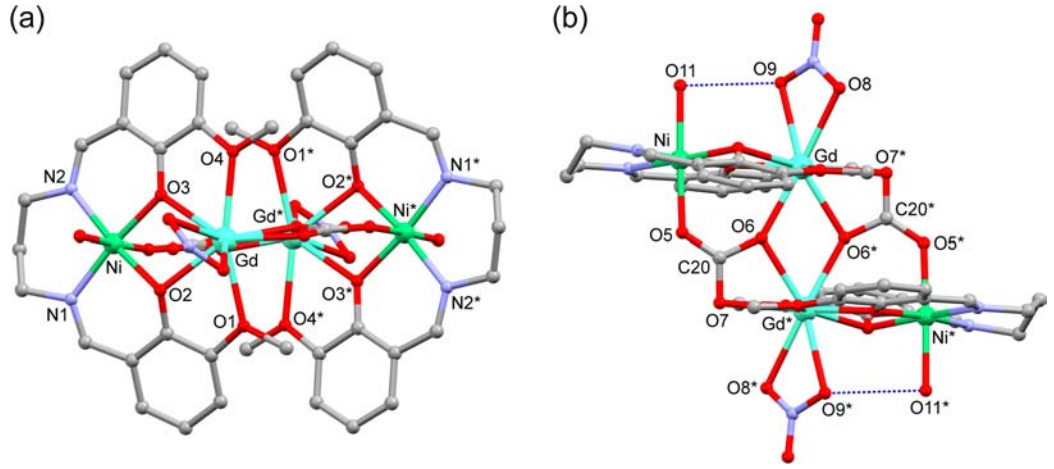

Figure 3. Molecular structures of the tetranuclear $Ni^{II}_2Gd^{III}_2$ complex **2Gd** with the selected atom numbering scheme. The tetranuclear molecule has an inversion center, and the hydrogen atoms are omitted for clarity. (a) Perspective view of **2Gd** projected on the N_2O_2 equatorial coordination planes. (b) Side view showing the $(\mu_4\text{-}CO_3)_2Ni^{II}_2Gd^{III}_2$ structure and the coordination of the H_2O to the Ni^{II} ion and of the chelating nitrate ligand to the Gd^{III} ion. Intramolecular hydrogen bond between H_2O and NO_3^-.

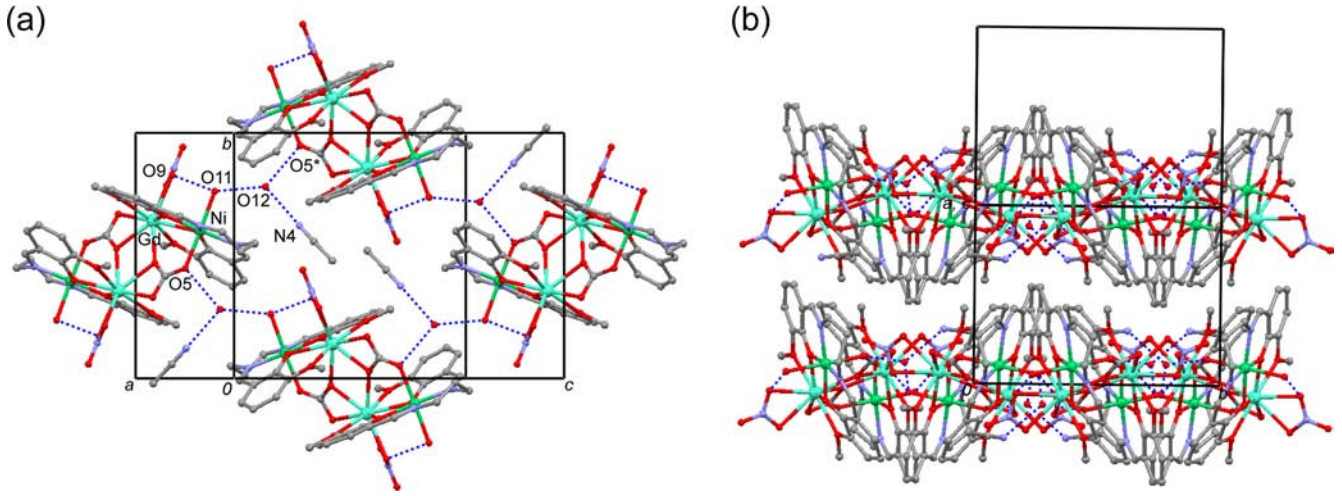

Figure 4. (a) Crystal structure of $Ni^{II}_2Ln^{III}_2$ complex **2Gd**, projected along the *a* axis. (b) Stacking of the adjacent 2D layers of **2Gd**.

and links one Ni and two Gd ions. The two Ni−O−Gd bridging angles in the NiO_2Gd unit are 104.1(3) and 103.4(3)°.

The high-spin Ni^{II} ion has an octahedral coordination environment formed by the N_2O_2 donor atoms of the 3-MeOsaltn ligand, with bond distances of Ni−O2 = 2.036(8) Å, Ni−O3 = 2.043(7) Å, Ni−N1 = 2.027(9) Å, and Ni−N2 = 2.042(9) Å in the equatorial plane. The two axial sites are occupied by an oxygen atom of the methanol ligand with a distance of Ni−O11 = 2.192(8) Å and one oxygen atom of the carbonate ion with a distance of Ni−O5 = 2.107(8) Å. The Ni−N and Ni−O bond distances and the coordination number of 6 are consistent with a high-spin state of the Ni^{II} ion ($S = 1$). The Gd^{III} ion is coordinated by the four oxygen atoms of two phenoxo and two methoxy oxygen atoms of {Ni^{II}(3-MeOsaltn)(MeOH)}, two oxygen atoms of the NO_3^- ion acting as a chelate ligand, with Gd−O8 = 2.457(8) Å and Gd−O9 = 2.514(9) Å, two oxygen atoms of a carbonato, with Gd*−O6 = 2.363(7) Å and Gd*−O7 = 2.462(7) Å, and one oxygen atom of another carbonato with Gd*−O6* = 2.349(7) Å; a coordination number of 9 is thus attained. The coordinated two oxygen atoms of the NO_3^- ion roughly lie on the Gd−O1 and Gd−O4 bonds (O1 and O4 are methoxy oxygen atoms) and the plane of the NO_3^- ion is declined to the outside.

Figure 2a shows the crystal structure projected along the *a* axis of **1Gd**, as a representative example of the crystal packing in the first series of complexes. The coordinated methanol oxygen atom O11 to the Ni^{II} ion is hydrogen-bonded to the oxygen atom O5 of the carbonate ion of the adjacent $Ni^{II}_2Gd^{III}_2$ molecule, with the hydrogen-bond distance O11···O5* = 2.844 Å (*, $-^1/_2 + x$, $^1/_2 - y$, $-^1/_2 + z$), to produce a two-dimensional layer structure, where a cyclic structure consisting of $(\cdots\{Ni^{II}_2Gd^{III}_2\}\cdots Ni^{II}\cdots)_2$ is the unit of the 2D layer, with four intermolecular Ni···Ni distances (6.314 Å) and two intramolecular Ni···Ni distances (8.267 Å). Figure 2b shows the stacking manner of the adjacent 2D layers.

The molecular structure of the tetranuclear $Ni^{II}_2Gd^{III}_2$ complex **2Gd** is shown in Figure 3a,b. The tetranuclear $(\mu_4\text{-}CO_3)_2Ni^{II}_2Gd^{III}_2$ structure is essentially similar to that of **1Gd** in the first series. It is worth noting that differences are seen in the axial coordination of the solvent molecule to the Ni^{II} ion, in the orientation of the saturated six-membered chelate rings, and in the orientation of the bidentate nitrate ligand to the Gd^{III} ion. The water molecule O11 coordinates to the Ni^{II} ion with

dx.doi.org/10.1021/ic4008312 | Inorg. Chem. 2013, 52, 7218−7229

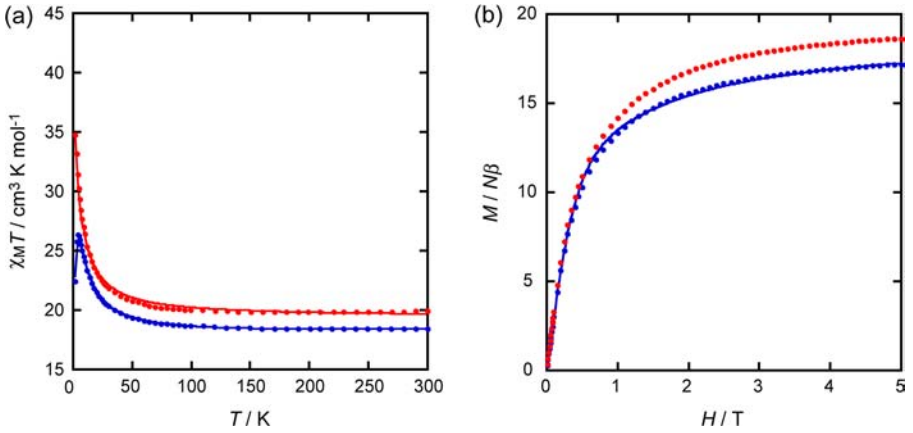

Figure 5. (a) Plots of $\chi_M T$ vs T for the $Ni^{II}_2Gd^{III}_2$ complexes **1Gd** (blue) and **2Gd** (red). The solid lines represent the theoretical curves with the best-fit parameters of g_{Ni} = 2.22, g_{Gd} = 2.01, J(Ni−Gd) = +1.1 cm^{-1}, J'(Gd−Gd) = −0.012 cm^{-1}, and D_{Ni} = +0.45 cm^{-1} for **1Gd** and g_{Ni} = 2.23, g_{Gd} = 2.07, J(Ni−Gd) = +1.0 cm^{-1}, J'(Gd−Gd) = +0.046 cm^{-1}, and D_{Ni} = +0.23 cm^{-1} for **2Gd**. (b) Field dependence of the magnetization at 1.9 K as the plots of $M/N\beta$ vs H for **1Gd** (blue) and **2Gd** (red). The black solid line represents the theoretical curve for **1Gd** with the best-fit parameters of $g_{9/2}$ = 2.19 and $D_{9/2}$ = +0.68 cm^{-1}.

the distance Ni−O11 = 2.137(3) Å, instead of methanol with the distance Ni−O11 = 2.192(8) Å in **1Gd**. As seen in Figures 1b and 3b, the orientation of two central carbon atoms of the two six-membered chelate rings in Ni^{II}(3-MeOsaltn) moieties is different between **1Gd** and **2Gd**. The two Gd−O coordination bond distances in **2Gd** are Gd−O2 = 2.353(3) Å and Gd−O3 = 2.315(3) Å, while those in **1Gd** are Gd−O2 = 2.344(7) Å and Gd−O3 = 2.358(7) Å. The coordinated water molecule O11 to the Ni^{II} ion in **2Gd** is hydrogen-bonded to the O9 of the nitrato coordinated to the Gd^{III} ion with distance O11···O9 = 2.924 Å. Because of this intramolecular hydrogen bond, the plane of the nitrato is rotated in the Ni ← Gd direction and the coordinated two oxygen atoms of the NO_3^- ion roughly lie in the direction of the Gd−O3 bond (O3 is phenoxy oxygen). The two Ni−O−Gd bridging angles of **2Gd** are 102.0(1)° for Ni−O2−Gd and 105.0(1)° for Ni−O3−Gd, showing a slightly higher asymmetry than those of **1Gd**, with the corresponding angles of 104.1(3) and 103.4(3)°. Examination of the Ni−O and Gd−O bond distances in the NiO_2Gd core also shows the higher asymmetry of **2Gd** than **1Gd**.

Figure 4a shows the crystal structure projected along the *a* axis of **2Gd**, as a representative example of the crystal packing in the isomorphous **2Gd**, **2Tb**, and **2Dy** series. Here, a crystal water molecule O12 is triply hydrogen-bonded to the oxygen atom O11 of the water molecule coordinated to the Ni^{II} ion, to the nitrogen atom N4 of an acetonitrile crystal solvent, and to the oxygen atom O5 of the carbonate ion, with the hydrogen-bond distances O12···O11 = 2.703 Å, O12···N4 = 2.895 Å, and O12···O5 = 2.770 Å, respectively. Adjacent $Ni^{II}_2Gd^{III}_2$ molecules, hydrogen-bonded via this crystal water O12, produce a 2D layer structure consisting of a cyclic structure $(\cdots(Ni^{II}_2Gd^{III}_2)\cdots H_2O\cdots)_4$ as the constituting unit. The intermolecular Ni···Ni distance of 7.621 Å is significantly longer than the corresponding distance of 6.314 Å in **1Gd**. Figure 4b shows the stacking manner of the adjacent 2D layers.

General Procedure of Magnetic Measurements of $Ni^{II}_2Ln^{III}_2$ Complexes. The temperature dependences of the magnetic susceptibilities for the two series of $Ni^{II}_2Ln^{III}_2$ complexes (**1Gd**, **1Tb**, and **1Dy**) and (**2Gd**, **2Tb**, and **2Dy**) were measured on powdered samples dispersed in paraffin grease in the temperature range of 1.9−300 K under 0.1 T. The corresponding field dependences of the magnetization were measured at 1.9 K. The ac magnetic susceptibility measurements were measured as a function of the temperature from 2 to 20 K in 0 and 1000 Oe applied dc field and 5 Oe oscillating field at frequencies 10−10000 Hz.

Magnetic Properties of $Ni^{II}_2Gd^{III}_2$. The plots of $\chi_M T$ vs T for the $Ni^{II}_2Gd^{III}_2$ complexes **1Gd** and **2Gd** are shown in Figure 5a. The magnetic susceptibilities followed the Curie−Weiss equation, $1/\chi_M = C(T - \theta)$, with θ = +2.3 K for **1Gd** and θ = +2.2 K for **2Gd**. The $\chi_M T$ values at 300 K were 18.43 and 19.88 cm^3 K mol^{-1} for **1Gd** and **2Gd**, respectively, whose values are slightly larger than the value of 17.76 cm^3 K mol^{-1} per $Ni^{II}_2Gd^{III}_2$ expected for high-spin Ni^{II} (S = 1) and Gd^{III} ($4f^7$, J = $^7/_2$, L = 0, S = $^7/_2$, $^8S_{7/2}$) noninteracting ions. Upon lowering of the temperature, the $\chi_M T$ value of **1Gd** increased gradually to reach a maximum of 26.33 cm^3 K mol^{-1} at 4.0 K and then slightly decreased. For **2Gd**, the $\chi_M T$ value monotonically increased, reaching a value of 34.86 cm^3 K mol^{-1} at 1.9 K. The increase of $\chi_M T$ upon lowering of the temperature indicates dominant intramolecular Ni^{II}−Gd^{III} ferromagnetic interactions, consistent with the positive Weiss constants. The slight decrease below 4.0 K of **1Gd** can be ascribed to a zero-field splitting (ZFS) of the Ni^{II} ion and/or to a small antiferromagnetic coupling between the Gd^{III} ions, while the increase of **2Gd** at the lowest-temperature region can be ascribed to a ferromagnetic coupling between the Gd^{III} ions.

Because the ground state of the Gd^{III} ion ($^8S_{7/2}$) has no contribution from orbital angular momentum, the magnetic susceptibility of this $Ni^{II}_2Gd^{III}_2$ complex can be reproduced by the equation derived from the following spin-only Hamiltonian for the tetranuclear spin structure on the basis of the molecular structure in Scheme 2:

$$\begin{aligned} H = {} & \beta(g_{Ni}\hat{S}_{Ni1} + g_{Gd}\hat{S}_{Gd1} + g_{Gd}\hat{S}_{Gd2} + g_{Ni}\hat{S}_{Ni2})\cdot H \\ & - 2J(\text{Ni}-\text{Gd})(\hat{S}_{Ni1}\cdot\hat{S}_{Gd1} + \hat{S}_{Ni2}\cdot\hat{S}_{Gd2}) \\ & - 2J'(\text{Gd}-\text{Gd})\hat{S}_{Gd1}\cdot\hat{S}_{Gd2} \\ & + D_{Ni}[\hat{S}_{zNi1}{}^2 - S(S+1)/3] \\ & + D_{Ni}[\hat{S}_{zNi2}{}^2 - S(S+1)/3] \end{aligned} \quad (1)$$

Here g_{Ni} and g_{Gd} are the g factors for the Ni^{II} and Gd^{III} ions, H is the applied field, D_{Ni} is the ZFS parameter for Ni^{II},

dx.doi.org/10.1021/ic4008312 | Inorg. Chem. 2013, 52, 7218−7229

Scheme 2. Tetranuclear Spin Structure Used in Magnetic Analysis of the $Ni^{II}_2Gd^{III}_2$ Complex

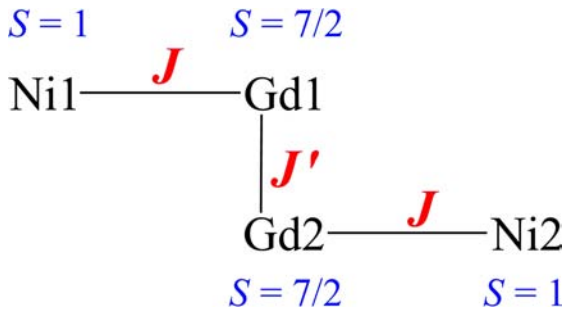

J(Ni−Gd) is the Heisenberg coupling constant between the Ni^{II} and Gd^{III} ions, and J'(Gd−Gd) is the Heisenberg coupling constant between the two adjacent Gd^{III} ions, while the intramolecular Ni^{II}−Ni^{II} magnetic interaction was neglected because of the much longer magnetic path. The magnetic susceptibility at each temperature was calculated using the theoretical equation $\chi = M/H = [N\sum_i(-dE_i/dH)\exp(-E_i/kT)]/[H\sum_i\exp(-E_i/kT)]$. The energy levels of the tetramer, E_i, were evaluated by diagonalizing the Hamiltonian matrix (with dimensions 576 × 576) in the uncoupled spin-function basis set. The best-fit parameters were $g_{Ni} = 2.22$, $g_{Gd} = 2.01$, J(Ni−Gd) = +1.1 cm^{-1}, J'(Gd−Gd) = −0.012 cm^{-1}, and D_{Ni} = +0.45 cm^{-1} for **1Gd** and $g_{Ni} = 2.23$, $g_{Gd} = 2.07$, J(Ni−Gd) = +1.0 cm^{-1}, J'(Gd−Gd) = +0.046 cm^{-1}, and D_{Ni} = +0.23 cm^{-1} for **2Gd** (see the solid lines in Figure 5a), indicating similar ferromagnetic Ni^{II}−Gd^{III} interactions and very small Gd^{III}−Gd^{III} interactions, antiferromagnetic in **1Gd** and ferromagnetic in **2Gd**. The values for g_{Ni} and D_{Ni} are in the range observed for the similar $Ni^{II}Ln^{III}$ complex,[18] and also the $Ni^{II}Gd^{III}$ coupling constants are in the range reported for analogous phenoxo-bridged $Ni^{II}Gd^{III}$ complexes.[19] Both antiferromagnetic[20a] and ferromagnetic[20b] coupling constants have been observed for oxyanion-bridged Gd^{III} dimers with small absolute values, below 0.1 cm^{-1}.[20] The change in the sign of J'(Gd−Gd) upon passing from **1Gd** to **2Gd** can be ascribed to their geometrical difference. These two compounds have the same $Ni^{II}_2Gd^{III}_2$ core, but the orientation of the bidentate ligand NO_3^-, Gd−Gd distance, and Gd−O−Gd angles show a slight difference.

The small magnetic interactions between the two central Gd^{III} ions indicate a "dimer of dimers" model with significant ferromagnetic coupling within the two [$Ni^{II}Gd^{III}$] binuclear subunits of the whole tetranuclear structure, constituting two weakly interacting $S = {}^9/_2$ spin states. The adequacy of this model is particularly evident for **1Gd**, for which the maximum value of 26.33 cm^3 K mol^{-1} at 4.0 K is only slightly higher than the value of 24.76 cm^3 K mol^{-1} expected for two isolated $S = {}^9/_2$ spin states resulting from ferromagnetic coupling between the Ni^{II} ($S = 1$) and Gd^{III} ($S = {}^7/_2$) ions within the two [$Ni^{II}Gd^{III}$] binuclear units. This "dimer of dimers" model is consistent with the field dependence of the magnetization as plots of $M/N\beta$ vs H (see Figure 5b), which show saturated magnetization values of 17.19 $N\beta$ for **1Gd** and 18.63 $N\beta$ for **2Gd**, around the expected value of 18 $N\beta$ (7 $N\beta$ for each of the Gd^{III} ions and 2 $N\beta$ for each of the two Ni^{II} ions), and can be qualitatively reproduced by Brillouin curves for two independent $S = {}^9/_2$ spin systems (see the dashed lines in Figure 5b). Indeed, considering the value of J(Ni−Gd) = +1.1 cm^{-1} for **1Gd** from the magnetic susceptibility analysis above, the lowest $S = {}^7/_2$ excited state is calculated to be 9.9 cm^{-1} (9 J) above the $S = {}^9/_2$ ground state and is thus not significantly populated at the temperature of 1.9 K at which the magnetization data have been measured, demonstrating that the $S = {}^9/_2$ spin ground state of each subunit is essentially isolated at this temperature. The data for **1Gd** can be quantitatively simulated including a ZFS term in the Hamiltonian $H = g_{9/2}\beta SH + D_{9/2}[S_z^2 - S(S+1)/3]$ in which $g_{9/2}$ and $D_{9/2}$ are the g factor and ZFS parameters for the $S = {}^9/_2$ state, and the best fit to the experimental data yields $g_{9/2} = 2.19$ and $D_{9/2}$ = +0.68 cm^{-1}; see the solid line in Figure 5b.

The $Ni^{II}_2Gd^{III}_2$ complexes **1Gd** and **2Gd** showed no frequency-dependent signals down to 2 K in the presence or absence of a 1000 Oe bias field, indicating no slow magnetic relaxation (Figure S2, Supporting Information).

Magnetic Properties of $Ni^{II}_2Tb^{III}_2$ Complexes. The plots of $\chi_M T$ vs T for **1Tb** and **2Tb** are shown in Figure 6a. The $\chi_M T$ values at 300 K for **1Tb** and **2Tb** are 26.38 and 27.77 cm^3 K mol^{-1}, respectively, which are slightly larger than the value of 25.84 cm^3 K mol^{-1} expected for two Ni^{II} ($S = 1$) and two Tb^{III} ($4f^8$, $J = 6$, $S = 3$, $L = 3$, $^7F_6$) noninteracting ions with $g_{Ni} = 2.00$ and $g_J = {}^3/_2$. Upon lowering of the temperature, the $\chi_M T$ value of **1Tb** slightly decreases, reaching a shallow minimum value of 25.87 cm^3 K mol^{-1} at 75 K, then gradually increases to reach a maximum value of 32.98 cm^3 K mol^{-1} at 6.0 K, and finally decreases abruptly to 20.99 cm^3 K mol^{-1} at 1.9 K. For

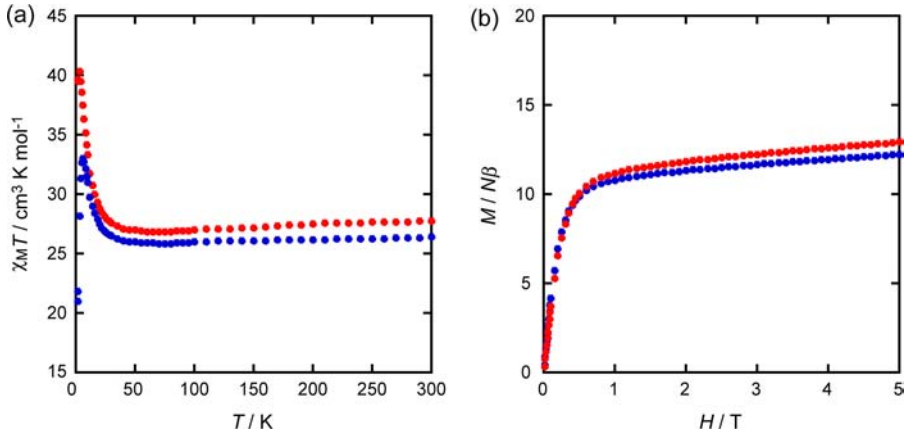

Figure 6. (a) Plots of $\chi_M T$ vs T for the $Ni^{II}_2Tb^{III}_2$ complexes **1Tb** (blue) and **2Tb** (red). (b) Field dependences of the magnetization at 1.9 K for **1Tb** (blue) and **2Tb** (red).

dx.doi.org/10.1021/ic4008312 | Inorg. Chem. 2013, 52, 7218−7229

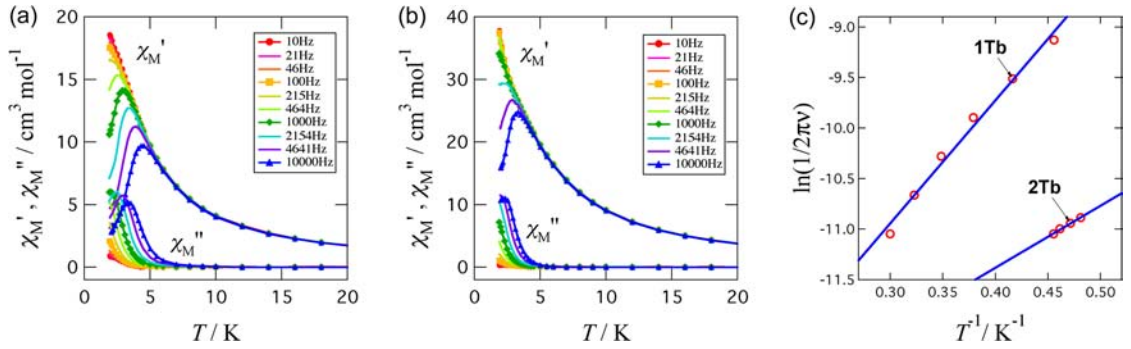

Figure 7. Temperature dependences of χ_M' and χ_M'' of (a) **1Tb** and (b) **2Tb** measured with a 1000 Oe external dc field. (c) Arrhenius plots. For the equation and optimized parameters, see the text.

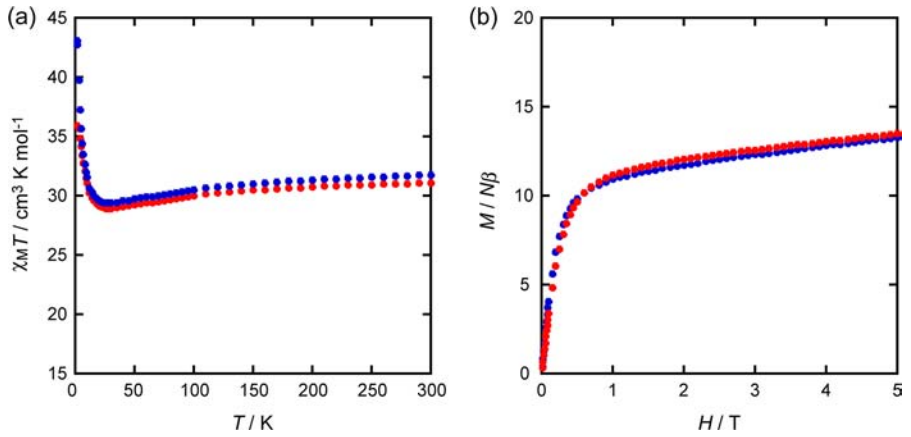

Figure 8. (a) Plots of $\chi_M T$ vs T for the $Ni^{II}_2Dy^{III}_2$ complexes **1Dy** (blue) and **2Dy** (red). (b) Field dependences of the magnetization at 1.9 K for **1Dy** (blue) and **2Dy** (red).

2Tb, the $\chi_M T$ value slightly decreases, reaching a shallow minimum of 26.85 cm^3 K mol^{-1} at 65 K, and then gradually increases to reach a maximum value of 40.37 cm^3 K mol^{-1} at 3.0 K, followed by a marginal decrease to 39.37 cm^3 K mol^{-1} at 1.9 K. It is noted that the apparent magnetic difference between **1Tb** and **2Tb** is observed in the $\chi_M T$ vs T plots at the lowest-temperature region.

As shown in Figure 6b, upon an increase of the applied external magnetic field to 5 T, the magnetizations of the $Ni^{II}_2Tb^{III}_2$ complexes **1Tb** and **2Tb** increase up to 12.24 and 12.93 $N\beta$, respectively, but did not reach the expected saturation value of 22 $N\beta$ (9 $N\beta$ for each of the Tb^{III} ions and 2 $N\beta$ for each of the two Ni^{II} ions). This is mostly due to the crystal-field effect on the Tb^{III} ion ($4f^8$, $J = 6$, $S = 3$, $L = 3$, $^7F_6$), which removes the 13-fold degeneracy of the $^7F_6$ ground state.[21]

Parts a and b of Figure 7 show the in-phase and out-of-phase portions of the ac susceptibility (χ_M' and χ_M'', respectively) for **1Tb** and **2Tb**, measured after a dc bias field of 1000 Oe was applied to reduce a possible quantum tunneling of the magnetization.[22] Upon cooling, an increase of χ_M'' was found together with a decrease of χ_M'. When we plotted the χ_M'' against χ_M' at various temperatures according to the Cole−Cole analysis[23] (Figure S3a in the Supporting Information), a semicircle was clearly drawn at each temperature. The α value is considerably small [$\alpha = 0.213(11)$ at 2 K and 0.21−0.12 at 2−5 K] in the Debye model, $\chi(\omega) = \chi_S + (\chi_T - \chi_S)/[1 + (i\omega\tau)^{1-\alpha}]$ where χ_T and χ_S are the isothermal and adiabatic susceptibilities, respectively.[22] This finding guarantees a single relaxation process for this complex. The Arrhenius plot[24] of **1Tb** shows a straight line for the χ_M'' peak (Figure 7c), and the activation energy (Δ) for the magnetization reversal was estimated as $\Delta/k_B = 12.2(7)$ K with $\tau_0 = 4.6(11) \times 10^{-7}$ s, where τ_0 stands for the preexponential factor in the Arrhenius equation, $\ln(2\pi\nu) = -\ln(\tau_0) - \Delta/k_BT$. The linear Arrhenius behavior down to 2 K indicates that the relaxation takes place mainly via thermal activation and that the quantum tunneling of the magnetization is practically negligible at the 1000 Oe dc bias field. A clear frequency dependence was also observed for **2Tb** at a 1000 Oe dc bias field, and the Cole−Cole plot is drawn, although the semicircle is incomplete (Figure S3b in the Supporting Information). The small α value was confirmed [0.16(2) at 2 K]. The peak of χ_M'' was found only around 2 K, and a meaningful Arrhenius plot was available after detailed measurements were performed around 2 K (Figure 7c).

Magnetic Properties of $Ni^{II}_2Dy^{III}_2$ Complexes. The plots of $\chi_M T$ vs T for **1Dy** and **2Dy** are shown in Figure 8a. The $\chi_M T$ values at 300 K for **1Dy** and **2Dy**, 31.77 and 31.11 cm^3 K mol^{-1}, are slightly larger than the value of 30.34 cm^3 K mol^{-1} expected for two Ni^{II} ($S = 1$) and two Dy^{III} ($4f^9$, $J = {}^{15}/_2$, $S = {}^5/_2$, $L = 5$, $^6H_{15/2}$) noninteracting ions with $g_{Ni} = 2$ and $g_J = {}^4/_3$. Upon lowering of the temperature, the $\chi_M T$ value of **1Dy** slightly decreases, reaching a shallow minimum of 29.39 cm^3 K mol^{-1} at 28 K, and then monotonically increases to reach the value of 43.10 cm^3 K mol^{-1} at 1.9 K. For **2Dy**, the $\chi_M T$ value gradually decreases, reaching a shallow minimum of 28.93 cm^3 K mol^{-1} at 30 K, and then increases to reach a maximum value of 35.96 cm^3 K mol^{-1} at 2 K.

dx.doi.org/10.1021/ic4008312 | Inorg. Chem. 2013, 52, 7218−7229

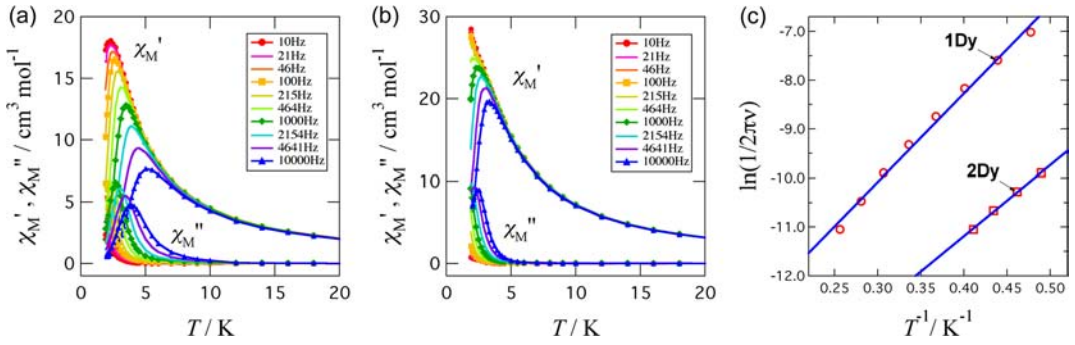

Figure 9. Temperature dependences of χ_M' and χ_M'' of (a) **1Dy** and (b) **2Dy** measured with a 1000 Oe external dc field. (c) Arrhenius plots. For the equation and optimized parameters, see the text.

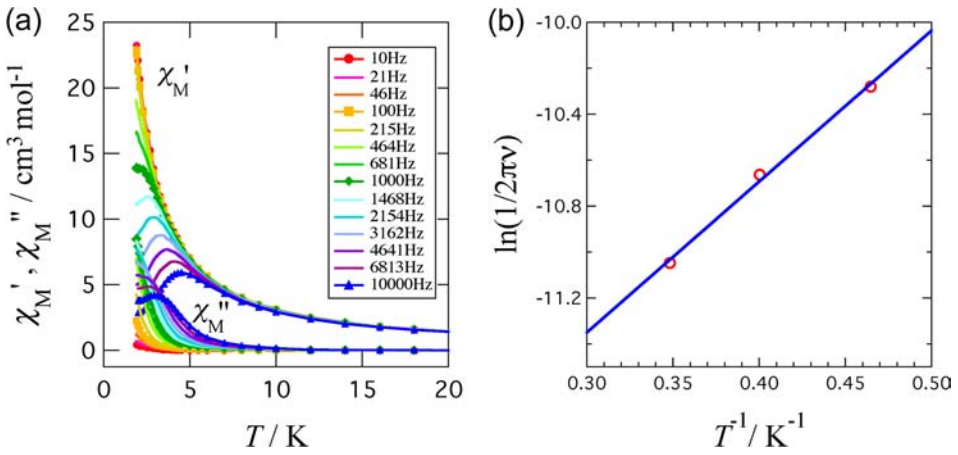

Figure 10. (a) Temperature dependences of χ_M' and χ_M'' of **1Dy** measured without any external dc field. (b) Arrhenius plot. For the equation and optimized parameters, see the text.

As shown in Figure 8b, upon an increase in the applied external magnetic field to 5 T, the magnetizations of **1Dy** and **2Dy** increase up to 13.29 and 13.48 $N\beta$, respectively, without reaching the expected saturation value of 24 $N\beta$ (10 $N\beta$ for each of the two Dy^{III} ions and 2 $N\beta$ for each of the two Ni^{II} ions). This is also mostly due to the crystal-field effect on the Dy^{III} ion ($4f^9$, $J = {}^{15}/_2$, $S = {}^{5}/_2$, $L = 5$, $^6H_{15/2}$), which removes the 16-fold degeneracy of the $^6H_{15/2}$ ground state.[21]

Parts a and b of Figure 9 display the ac susceptibility results for **1Dy** and **2Dy**, respectively, measured at a dc bias field of 1000 Oe. The Cole−Cole plots showed a semicircle (Figure S3c,d in the Supporting Information), with the α values considerably small [α = 0.206(6) and 0.154(7) for **1Dy** and **2Dy**, respectively, at 2 K]. The Arrhenius plots of **1Dy** and **2Dy** showed a linear relationship for each χ_M'' peak (Figure 10b), and the activation energies for the magnetization reversal were estimated as Δ/k_B = 18.1(6) K with $\tau_0 = 1.8(4) \times 10^{-7}$ s for **1Dy** and Δ/k_B = 14.5(4) K with $\tau_0 = 4.2(8) \times 10^{-8}$ s for **2Dy**. Interestingly, **1Dy** showed relatively slow relaxation of magnetization reorientation even at zero dc applied field (Figure 10). A meaningful Cole−Cole plot was drawn (Figure S3e in the Supporting Information). The linear Arrhenius plot down to 2 K gave Δ/k_B = 6.6(4) K with $\tau_0 = 1.6(3) \times 10^{-6}$ s (Figure 9c).

SMM Parameters of $Ni^{II}_2Ln^{III}_2$ Complexes. These SMM characteristics are summarized in Table 3. The $Ni^{II}_2Dy^{III}_2$ compounds showed higher Δ than the $Ni^{II}_2Tb^{III}_2$ compounds. It may be related that the Dy^{III} ion is a Kramers ion but Tb^{III} is not. The former inherently possesses a ground doublet state,

Table 3. ac Magnetic Susceptibility Results on the $Ni^{II}_2Ln^{III}_2$ Complexes

	1Tb	2Tb	1Dy	2Dy	1Dy
H_{dc}	1000	1000	1000	1000	0
Δk_B^{-1}/K[a]	12.2(7)	6.1(3)	18.1(6)	14.5(4)	6.6(4)
τ_0/s[a]	$4.6(11) \times 10^{-7}$	$9.7(15) \times 10^{-7}$	$1.8(4) \times 10^{-7}$	$4.2(8) \times 10^{-8}$	$1.6(3) \times 10^{-6}$
α[b]	0.213(11)	0.16(2)	0.206(6)	0.154(7)	0.161(12)

[a]From the Arrhenius plot using the χ_M'' peaks. [b]From the Cole−Cole plot measured at 2.0 K. For the equation, see the text.

favoring the double-well potential surface suitable for the Arrhenius behavior. A similar advantage in the activation energy for Dy analogues over Tb analogues has often been observed for polynuclear Ln^{III} systems[10] and heterodinuclear $Cu^{II}Ln^{III}$ systems involving Schiff-base ligands.[25,26] As a comparison between the **1Ln** and **2Ln** series, we can find that the former seems to be better in the SMM development because the Δ values of **1Ln** are somewhat larger than those of **2Ln**. This may be related to the magnetic anisotropy of Ln^{III}.[27] All of the present Tb and Dy compounds showed SMM behavior, probably being assisted by the ferromagnetic Ni−Tb and Ni−Dy couplings. The ground high-spin state is a requirement of SMMs,[23] and it has been realized in the present compounds, as indicated by the increase in $\chi_M T$ upon lowering of the temperature for all of them. Therefore, the ground molecular design of $Ni^{II}Ln^{III}$ is generally successful, although the magnetic anisotropy of Ln^{III} and the Ln−Ln magnetic interaction are

dx.doi.org/10.1021/ic4008312 | Inorg. Chem. 2013, 52, 7218−7229

somewhat uncontrollable. Further studies of the synthetic, structural, and magnetic properties on the analogous compounds and DFT and ab initio calculations of Ln−Ni exchange parameters are undertaken to elucidate the details.

■ ASSOCIATED CONTENT

Supporting Information

Photographs of crystals (Figure S1), temperature dependences (Figure S2), Cole−Cole plots (Figure S3), and X-ray crystallographic files (CIF) for compounds **1Gd**, **1Tb**, **1Dy**, **2Gd**, **2Tb**, and **2Dy**. This material is available free of charge via the Internet at http://pubs.acs.org. Crystallographic files (CCDC 928513−928518) are also available upon application to the Cambridge Crystallographic Data Centre, 12 Union Road, Cambridge CB2 1EZ, U.K. [fax (+44)1223-336-033; e-mail deposit@ccdc.cam.ac.uk].

■ AUTHOR INFORMATION

Corresponding Author

*E-mail: naohide@aster.sci.kumamoto-u.ac.jp. Fax: +81-96-342-3390.

Notes

The authors declare no competing financial interest.

■ ACKNOWLEDGMENTS

T.F. and K.N. were supported by Research Fellowships of the Japan Society for the Promotion of Science, KAKENHI 00248556 and 00248498.

■ REFERENCES

(1) (a) Palner, D. A.; Eldik, R. V. *Chem. Rev.* **1983**, *83*, 651−731. (b) Floriani, C. *Pure Appl. Chem.* **1982**, *54*, 59−64. (c) Yin, X.; Moss, J. R. *Coord. Chem. Rev.* **1999**, *181*, 27−59. (d) Kkelsen, M. M.; Jorgensen, M.; Krebs, F. C. *Energy Environ. Sci.* **2010**, *3*, 43−81.

(2) (a) Nair, S. K.; Christianson, D. *J. Am. Chem. Soc.* **1991**, *113*, 9455−9458. (b) Sola, M.; Lledos, A.; Duran, M. *J. Am. Chem. Soc.* **1992**, *114*, 869−877. (c) Zhang, Y. J.; Men, K. M. *J. Am. Chem. Soc.* **1992**, *114*, 10498−10507.

(3) (a) Kato, M.; Ito, T. *Inorg. Chem.* **1985**, *24*, 504−508. (b) Churchill, M. R.; Davies, G.; El-Sayed, M. A.; El-Shazly, M. F.; Huchinson, J. P.; Rupich, M. W. *Inorg. Chem.* **1980**, *19*, 201−208. (c) Harada, H.; Kodera, M.; Vuckovic, G.; Matsumoto, N.; Kida, S. *Inorg. Chem.* **1991**, *30*, 1190−1194.

(4) (a) Kitajima, N.; Fujisawa, K.; Koda, T.; Hikichi, S.; Moro-oka, Y. *Chem. Commun.* **1990**, 1357−1358. (b) Tanase, T.; Nitta, S.; Yoshikawa, S.; Kobayashi, K.; Sakurai, T.; Yano, S. *Inorg. Chem.* **1992**, *31*, 1058−1062. (c) El-Hendawy, M. M.; English, N. J.; Mooney, D. A. *Inorg. Chem.* **2012**, *51*, 5282−5288. (d) Ito, M.; Takita, Y. *Chem. Lett.* **1996**, 929−930.

(5) (a) Ke, H.; Zhao, L.; Xu, G.-F.; Guo, Y.-N.; Tang, J.; Zhang, X.-Y.; Zhang, H.-J. *Dalton Trans.* **2009**, 10609−10613. (b) Bian, S.-D.; Jia, J.-H.; Wang, Q.-M. *J. Am. Chem. Soc.* **2009**, *113*, 3422−3423. (c) Langley, S. K.; Moubaraki, B.; Murray, K. S. *Inorg. Chem.* **2012**, *51*, 3947−3949. (d) Tian, H.; Zhao, L.; Guo, Y. N.; Guo, Y.; Tang, J.; Liu, Z. *Chem. Commun.* **2012**, *48*, 708−710. (e) Gass, I. A.; Moubaraki, B.; Langley, S. K.; Batten, S. R.; Murray, K. S. *Chem. Commun.* **2012**, *48*, 2089−2091.

(6) (a) Osa, S.; Kido, T.; Matsumoto, N.; Re, N.; Pochaba, A.; Mronzinski, J. *J. Am. Chem. Soc.* **2004**, *126*, 420−421. (b) Kido, T.; Ikuta, Y.; Sunatsuki, Y.; Ogawa, Y.; Matsumoto, N.; Re, N. *Inorg. Chem.* **2003**, *42*, 398−408. (c) Hamamatsu, T.; Yabe, K.; Towatari, M.; Matsumoto, N.; Re, N.; Pochaba, A.; Mrozinski, J. *Bull. Chem. Soc. Jpn.* **2007**, *80*, 523−529. (d) Hamamatsu, T.; Yabe, K.; Towatari, M.; Osa, S.; Matsumoto, N.; Re, N.; Pochaba, A.; Mrozinski, J.; Gallani, J. L.; Barla, A.; Imperia, P.; Paulsen, C.; Kappler, J. P. *Inorg. Chem.* **2007**, *46*, 4458−4468.

(7) (a) Towatari, M.; Hamamatsu, T.; Yabe, K.; Matsumoto, N.; Mrozinski, J. *Proceedings of the XVth Winter School on Coordination Chemistry*, Karpacz, Poland, Dec 4−8, 2006. They reported complexes $[Cu^{II}(3\text{-MeOsaltn})(ac)Ln^{III}(hfac)_2]$ (Ln^{III} = Gd^{III}, Dy^{III}, Tb^{III}). (b) Towatari, M.; Nishi, K.; Fujinami, T.; Matsumoto, N.; Mochida, N.; Ishida, T.; Sunatsuki, Y.; Kojima, M.; Re, N.; Mrozinski, J. *Inorg. Chem.* **2013**, *52* (10), 6160−6178.

(8) (a) Wang, J.-H.; Yan, P. F.; Li, G. M.; Zhang, J. W.; Chen, P.; Suda, M.; Einaga, Y. *Inorg. Chim. Acta* **2010**, *363*, 3706−3713. (b) Pasatoiu, T. D.; Tiseanu, C.; Madalan, A. M.; Jurca, B.; Duhayon, C.; Sutter, J. P.; Andruh, M. *Inorg. Chem.* **2011**, *50*, 5890−5898.

(9) (a) Sessoli, R.; Gatteschi, D.; Caneschi, A.; Novak, M. A. *Nature* **1993**, *365*, 141−143. (b) Gatteschi, D.; Caneschi, A.; Pardi, L.; Sessoli, R. *Science* **1994**, *265*, 1054−1058. (c) Sessoli, R.; Tsai, H. L.; Schake, A. R.; Wang, S.; Vincent, J. B.; Folting, K.; Gatteschi, D.; Christou, G.; Hendrickson, D. N. *J. Am. Chem. Soc.* **1993**, *115*, 1804−1816. (d) Boskovic, C.; Brechin, E. K.; Streib, W. E.; Folting, K.; Bollinger, J. C.; Hendrickson, D. N.; Christou, G. *J. Am. Chem. Soc.* **2002**, *124*, 3725−3736.

(10) (a) Zhang, P.; Guo, Y.-N.; Tang, J. *Coord. Chem. Rev.* **2013**, *257*, 1728−1763. (b) Habib, F.; Murugesu, M. *Chem. Soc. Rev.* **2013**, *42*, 3278−3288.

(11) (a) Costes, J. P.; Vendier, L.; Wernsdorfer, W. *Dalton Trans.* **2011**, *40*, 1700−1706. (b) Ferbinteanu, M.; Kajiwara, T.; Choi, K. Y.; Nojiri, H.; Nakamoto, A.; Kojima, N.; Cimpoesu, F.; Fujimura, Y.; Takaishi, S.; Yamashita, M. *J. Am. Chem. Soc.* **2006**, *128*, 9008−9009. (c) Mori, F.; Nyui, T.; Ishida, T.; Nogami, T.; Choi, K.-Y.; Nojiri, H. *J. Am. Chem. Soc.* **2006**, *128*, 14408−14009. (d) Gao, Y.; Zhao, L.; Xu, X.; Xu, G.-F.; Guo, Y.-N.; Tang, J.; Liu, Z. *Inorg. Chem.* **2011**, *50*, 1304−1308. (e) Colacio, E.; Ruiz, J.; Mota, A. J.; Palacios, M. A.; Cremades, E.; Ruiz, E.; White, F. J.; Brechin, E. K. *Inorg. Chem.* **2012**, *51*, 5857−5868. (f) Efthymiou, C. G.; Stamatatos, T. C.; Papatriantafyllopoulou, C.; Tasiopoulos, A. J.; Wernsdorfer, W.; Perlepes, S. P.; Christou, G. *Inorg. Chem.* **2010**, *49*, 9737−9739. (g) Feltham, H. L. C.; Lan, Y.; Klower, F.; Ungur, L.; Chibotaru, L. F.; Powell, A. K.; Brooker, S. *Chem.—Eur. J.* **2011**, *17*, 4362−4365.

(12) Sakamoto, S.; Yamauchi, S.; Hagiwara, H.; Matsumoto, N.; Sunatsuki, Y.; Re, N. *Inorg. Chem. Commun.* **2012**, *26*, 20−23.

(13) Gruber, S. J.; Harris, C. M.; Sinn, E. *J. Inorg. Nucl. Chem.* **1968**, *30*, 1805−1830.

(14) Kahn, O. *Molecular Magnetism*; VCH: Weinheim, Germany, 1993; Chapter 1, Table I.1.

(15) *Crystalstructure 3.7.0, Crystal Structure Analysis Package*; Rigaku and Rigaku/MSC: The Woodlands TX, 2000−2005.

(16) Sheldrick, G. M. *SHELXL-97*; University of Göttingen: Göttingen, Germany, 1997.

(17) Nakamoto, K. *Infrared and Raman Spectra of Inorganic and Coordination Compounds*, 2nd ed.; Wiley-Interscience: New York, 1970; p 98.

(18) Yamaguchi, T.; Sunatsuki, Y.; Ishida, H.; Kojima, M.; Akashi, H.; Re, N.; Matsumoto, N.; Pochaba, A.; Mrozinski, J. *Inorg. Chem.* **2008**, *47*, 5736−5745.

(19) (a) Costes, J.-P.; Dahan, F.; Dupuis, A.; Laurent, J.-P. *Inorg. Chem.* **1997**, *36*, 4284−4286. (b) Chen, Q.-Y.; Luo, Q.-H.; Zheng, L.-M.; Wang, Z.-L.; Chen, J.-T. *Inorg. Chem.* **2002**, *41*, 605−609. (c) Shiga, T.; Ito, N.; Hidaka, A.; Okawa, H.; Kitagawa, S.; Ohba, M. *Inorg. Chem.* **2007**, *46*, 3492−3501. (d) Chandrasekhar, V.; Pandian, B. M.; Boomishankar, R.; Steiner, A.; Vittal, J.; Houri, A.; Clerac, R. *Inorg. Chem.* **2008**, *47*, 4918−4929.

(20) (a) Panagiotopoulos, A.; Zafiropoulos, T. F.; Perlepes, S. P.; Bakalbassis, E.; Masson-Ramade, I.; Kahn, O.; Terzis, A.; Raptopoulou, C. P. *Inorg. Chem.* **1995**, *34*, 4918−4920. (b) Rizzi, A.; Baggio, R.; Calvo, R.; Garland, M. T.; Peña, O.; Perec, M. *Inorg. Chem.* **2001**, *40*, 3623−3625. (c) Rohde, A.; Urland, W. J. *Z. Anorg. Allg. Chem.* **2005**, *631*, 417−420. (d) Hatscher, S. T.; Urland, W. *Angew. Chem., Int. Ed.* **2003**, *42*, 2862−2864.

(21) (a) Kahn, O. *Molecular Magnetism*; VCH: Weinheim, Germany, 1993; Chapter 3.5. (b) Stevens, K. W. H. *Proc. Phys. Soc. London* **1952**, *A65*, 209.
(22) (a) Castro, S. L.; Sun, Z.; Grant, C. M.; Bollinger, J. C.; Hendrickson, D. N.; Christou, G. *J. Am. Chem. Soc.* **1998**, *120*, 2365−2375. (b) Ako, A. M.; Mereacre, M.; Hewitt, I. J.; Clerac, R.; Lecren, L.; Anson, C. E.; Powell, A. K. *J. Mater. Chem.* **2006**, *16*, 2579−2586. (c) Okazawa, A.; Nojiri, H.; Ishida, T.; Kojima, N. *Polyhedron* **2011**, *30*, 3140−3144. (d) Kajiwara, T.; Nakano, M.; Takaishi, S.; Yamashita, M. *Inorg. Chem.* **2008**, *47*, 8604−8606.
(23) Cole, K. S.; Cole, H. R. *J. Chem. Phys.* **1941**, *9*, 341−351.
(24) Sessoli, R.; Powell, A. K. *Coord. Chem. Rev.* **2009**, *253*, 2328−2341.
(25) (a) Gatteschi, D.; Sessoli, R.; Villain, J. *Molecular Nanomagnets*; Oxford University Press: New York, 2006. (b) Gatteschi, D.; Sessoli, R. *Angew. Chem., Int. Ed.* **2003**, *42*, 268−297.
(26) (a) Costes, J.-P.; Dahan, F.; Wernsdorfer, W. *Inorg. Chem.* **2006**, *45*, 5−7. (b) Kajiwara, T.; Nakano, M.; Takahashi, K.; Takaishi, S.; Yamashita, M. *Chem.—Eur. J.* **2011**, *17*, 196−205. (c) Kajiwara, T.; Takahashi, K.; Hiraizumi, T.; Takaishi, S.; Yamashita, M. *Polyhedron* **2009**, *28*, 1860−1863.
(27) Ishida, T.; Watanabe, R.; Fujiwara, K.; Okazawa, A.; Kojima, N.; Tanaka, G.; Yoshii, S.; Noriji, H. *Dalton Trans.* **2012**, *41*, 13609−13619.